IOP Publishing Nanotechnology
Nanotechnology 29 (2018) 385602 (5pp) https://doi.org/10.1088/1361-6528/aacfd7

Nitrogen anion-decorated cobalt tungsten disulfides solid solutions on the carbon nanofibers for water splitting

Meng Wan[1], Jiang Li[1], Tao Li[1], Han Zhu[1,2], Weiwei Wu[3] and Mingliang Du[1,2,4]

[1] College of Materials and Textiles, Key Laboratory of Advanced Textile Materials and Manufacturing Technology of the Ministry of Education, Zhejiang Sci-Tech University, Hangzhou, 310018, People's Republic of China
[2] Key Laboratory of Synthetic and Biological Colloids, Ministry of Education, School of Chemical and Material Engineering, Jiangnan University, Wuxi 214122, People's Republic of China
[3] School of Advanced Materials and Nanotechnology, Xidian University, Shaanxi, 710126, People's Republic of China

E-mail: du@jiangnan.edu.cn

Received 25 April 2018, revised 20 June 2018
Accepted for publication 28 June 2018
Published 11 July 2018

Abstract

A facile method to prepare nitrogen anion-decorated cobalt tungsten disulfides solid solutions, retaining ultra-thin WS_2-like nanosheet structures (The N–$Co_xW_{1-x}S_2$) anchored on carbon nanofibers (CNFs), is developed. The synergistic effect of the WS_2 nanosheets provides a secure framework for stabilizing the amorphous Co–S clusters, CNFs substrate and nitrogen anion-decoration significantly enhances the inherent conductivity of the catalyst, resulting in a significantly promoted hydrogen evolution reaction activity and stable performance compared to pure Co_9S_8 nanoparticles or ultra-thin WS_2 nanosheets. The N–$Co_xW_{1-x}S_2$ electrode demonstrates the excellent electrocatalytic performance, with current density of 10 mA cm^{-2} at a low overpotential of 93 mV and Tafel slope of 85 mV dec^{-1}, as well as the long-term stability in acid electrolyte. The present investigation may provide a feasible strategy for incorporating other heteroatoms into transitional metal disulfides materials to design catalysts with highly active and stable performance for water splitting.

Supplementary material for this article is available online

Keywords: solid solutions, water splitting, electrospinning, carbon nanofibers, hydrogen energy

(Some figures may appear in colour only in the online journal)

1. Introduction

The increasing depletion of traditional fossil fuels impels researchers to develop eco-friendly and renewable resources, to alleviate the energy crisis and environmental pollution hazards [1, 2]. Hydrogen, with high energy density, could be a potential alternative to fossil fuels as a clean and renewable resource. Water electrolysis is one of the most sustainable and cleanest methods for the production of hydrogen through hydrogen evolution reaction (HER) [3–5]. To date, Pt is still the most active HER catalyst, but the scarcity and high cost severely limit its practical applications [6–8]. Therefore, it is crucial to develop Pt-free electrocatalysts with earth-abundant elements while maintaining comparable HER performance to Pt.

Recently, considerable effort has been devoted to developing earth-abundant electrocatalysts and TMDs which have been recognized as the promising alternatives to noble metal catalysts [9–13]. WS_2, similar to MoS_2, is one of the most efficient two-dimensional TMDs and is widely used for the HER application [14]. However, the HER performance is

[4] Author to whom any correspondence should be addressed.

limited by the low electrical conductivity and insufficient active sites, which are mainly located at the edges [15, 16]. Therefore, numerous methods have been developed to either increase the number of active edge sites or activate the inert basal planes. Another effective alternative is to increase the electrical conductivity to facilitate charge transport by coupling with various conductive supports [17, 18], e.g., growing nanolayer WS_2 nanosheets on Au foils [19], preparing a WS_2/graphene hybrid structure [20] and growing MoS_2@Ni core/shell nanostructures on carbon cloth [21]. Therefore, it is important to not only increase the active sites but also improve the electrical conductivity at the same time for higher HER performance.

Introducing heteroatoms into MoS_2 or WS_2 can increase the HER catalytic activity typically because of the significantly decreased Gibbs free energy of hydrogen adsorption [22–24]. It has been documented that forming a solid solution of M_{II}(M = Co, Ni)WS can not only increase the HER activity but also improve the stability [25, 26]. Tran *et al* indicated that the catalytic active sites are located at $M_{II}S$ cluster in the single Co–S–W phase, while the WS_2 layer functions as a coordination ligand stabilizing and tuning the catalytic performance [27]. What's more, nitrogen anion-decoration may be an efficient way to enhance the electrical conductivity of the catalysts and expedite electron transfer during HER due to the fact that the TMDs nitrides were reported to be classical metallic or half-metallic materials with high electrical conductivity [23, 28, 29]. Chen *et al* took the metallic pyrite CoS_2 as a proof-of-concept study and rationally develop nitrogen anion-decorated CoS_2 porous nanowire arrays for the first time, serving as the high-active electrocatalyst for HER [30].

So far, although there has been some progress in improving the catalytic activity of CoS_2 by heteroatom metal doping, it is well recognized that the further improvement of the catalytic activity for CoS_2 material has still been largely limited due to the low surface active sites and inferior reaction dynamics. Therefore, developing an effective and all-in-one way to enhance the conductivity and stability is valuable and desirable. In this work, we report the facile synthesis of nitrogen anion-decorated CoWS solid solution nanosheets on carbon nanofibers (CNFs) through a combination of electrospinning and post-carbonization. The as-prepared catalyst can be directly used as the binder-free electrode for the HER application. The composite catalyst displays a low overpotential of 93 mV to reach a current density of 10 mA cm^{-2} and excellent long-term stability. It is proposed that the improved HER performance originates from the increased active sites, the formation of the solid solution and electrical conductivity. The present synthetic method can be easily scaled-up for industrial applications.

2. Experimental section

2.1. Preparation of N–$Co_xW_{1-x}S_2$ nanosheets on CNFs

The N–$Co_xW_{1-x}S_2$ nanosheets on CNF were prepared through electrospinning and post-carbonization. In a typical procedure, 0.2845 g of cobalt nitrate ($Co(NO_3)_2$) in 7.0 ml of N,N-Dimethylformamide (DMF) was slowly added into 8.0 ml of DMF containing 0.2845 g of ammonium metatungstate $(NH_4)_6H_2W_{12}O_{40}$ with continuous stirring, followed by addition of 1.930 g of polyacrylonitrile (PAN) powder. The above mixed solution was then transferred to a medical syringe. The electrospinning process was conducted at 18.0 kV, and the distance between the syringe needle tip and aluminum foil was kept 15.0 cm. The feeding rate was 0.5 ml h^{-1} and the humidity was controlled to be 40%–50%. After electrospinning, the as-formed precursor mats were peeled from the aluminum foil and transferred to an aluminum boat, which was placed in the center of a quartz tube. 0.5 g of sulfur powder in another alumina boat was placed in the upstream side. The quartz tube was then heated to 280 °C at a rate of 5 °C min^{-1} and kept for 3 h in Ar (120 sccm). The temperature was then increased to 600 °C and hold for 0.5 h, and further increased to 900 °C and kept for another 3 h. For comparison, Co_9S_8 and WS_2 were prepared with the same method. The as-prepared catalysis was directly used for binder-free electrodes.

2.2. Characterization

The morphology of the as-prepared samples was examined by a Zeiss Ultra 500 scanning electron microscope (SEM) at an acceleration voltage of 3.0 kV. The transmission electron microscope (TEM) images were taken at a JEOL JEM 2100F at 200 kV. The elemental composition distribution of catalyst were analyzed by high angle annular dark field scanning transmission electron microscope (STEM) and electron dispersion spectroscopy (EDS) at a Tecnai G2 F30 S-Twin, Philips-FEI at the acceleration voltage of 300 kV. The x-ray diffraction (XRD) patterns were recorded on a Bruker AXS D8 XRD instrument. The Raman spectras were acquired on a Renishaw invia spectrometer. The chemical states of the catalysts were characterized by x-ray photoelectron spectrometer (XPS) using Escalab 250Xi instrument with a monochromatic Al Kα source (1486.6 eV).

2.3. Electrochemical measurements

The electrocatalytic performance of as-prepared catalysts was evaluated using a standard three-electrode configuration. All the measurements were conducted on a CHI660E electrochemical work station in 0.50 M H_2SO_4 solution with a graphite rod and Ag/AgCl as the counter and the reference electrode, respectively. All the samples were cut into the regular size with fixed area of 0.5 cm × 0.5 cm and directly used as the working electrode. During the tests, the electrolyte solution was continuously bubbled with Ar gas. Cyclic voltammetry was carried out in the range of −0.265–0.556 V at scan rate of 5 mV s^{-1} to clean the catalyst surface. Line sweep voltammetry (LSV) was performed from 0.2 V to −0.8 V (versus which reference electrode) at scan rate of 2 mV s^{-1}. Electrochemical impedance spectroscopy (EIS) was conducted at potential of −0.23 V versus reversible hydrogen electrode in the frequency of 5–10 MHz.

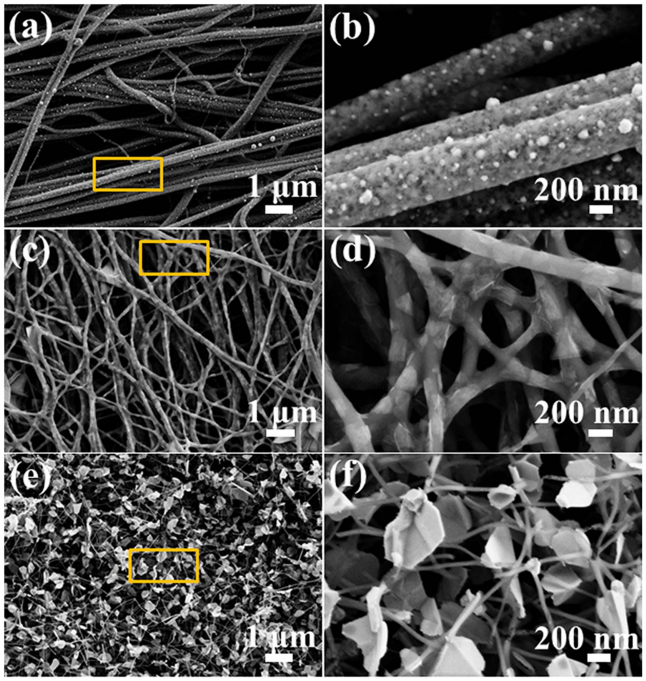

Figure 1. The low-magnification SEM images and the corresponding high-magnification SEM images of the yellow marked area of (a), (b) Co_9S_8, (c), (d) WS_2 and (e), (f) N–$Co_xW_{1-x}S_2$.

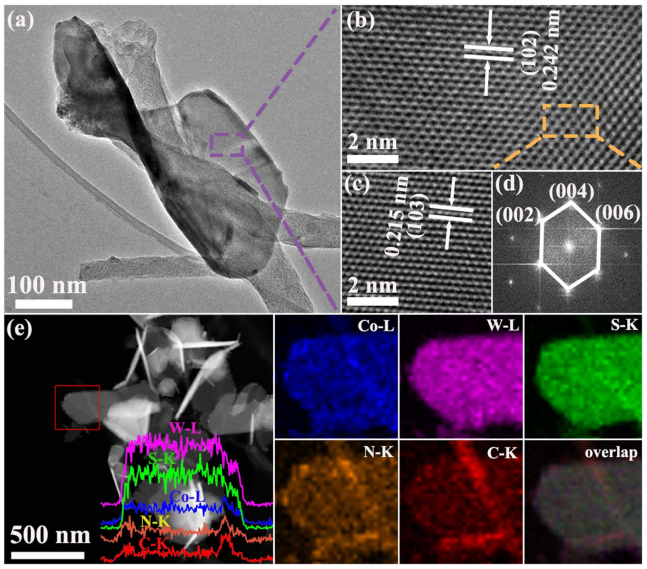

Figure 2. (a) The TEM image of N–$Co_xW_{1-x}S_2$ nanoflakes. (b), (c) HRTEM images marked the purple area in figure 2(a). (d) FFT partner obtained from the yellow area in figure 2(b). (e) The line-scan and element mapping of the N–$Co_xW_{1-x}S_2$ nanoflakes.

3. Results and discussion

Figure S1(a), available online at stacks.iop.org/NANO/29/385602/mmedia, shows the XRD patterns of as-prepared WS_2, Co_9S_8 and N–$Co_xW_{1-x}S_2$. The as-prepared WS_2 and Co_9S_8 were assigned to the hexagonal (JCPDS No. 08-0237) and cubic phase (JCPDS No. 19-0364), respectively. Compared with pure WS_2, the diffraction peaks of N–$Co_xW_{1-x}S_2$ have slight shifts to the higher-angle side because of the cell shrinkage caused by the smaller ionic radius of Co^{2+} (0.65 Å) compared to that of W^{4+} (0.74 Å) [31].

The results of the Raman characterization are displayed in figure S1(b). All three samples show two peaks located at 1337 and 1587 cm^{-1}, which are assigned to the D and G band of graphitized carbon, respectively [32]. The carbonization process successfully converted the organic polymer to graphitized carbon, which has high a electrical conductivity. Similar with the results of the XRD characterization, WS_2 and N–$Co_xW_{1-x}S_2$ show similar Raman spectral profiles, and both catalysts display vibrational peaks at approximately 350 and 417 cm^{-1}, which are the characteristic E_{2g} and A_{1g} vibration modes of WS_2 [33, 34]. Both the XRD and Raman characterization results suggest that as-synthesized N–$Co_xW_{1-x}S_2$ has a similar hexagonal phase to WS_2.

The morphology of the as-synthesized samples is characterized by SEM, as shown in figure 1. Co_9S_8 shows a particulate morphology with nanoparticles uniformly distributed on CNFs (figures 1(a) and (b)). WS_2 has a nanosheet structure that is intimately and horizontally attached to the CNFs (figures 1(c) and (d)). N–$Co_xW_{1-x}S_2$ ultra-thin nanosheets on CNFs show a hierarchical structure and stretch out the CNFs (figures 1(e) and (f)). The results of SEM-EDS indicate that the solid solutions have a formula of $Co_{0.85}W_{1.0}S_{2.75}$ (figure S2).

As shown in figure 2(a), the TEM image confirmed the hierarchical structure. The distance of the lattice fringes in figures 2(b) and (c) were measured to be 0.242 nm and 0.215 nm, matching the lattice distance of the (102) and (103) planes of hexagonal WS_2 with 0.249 nm for (102) and 0.227 nm for (103), respectively. In addition, the FFT image in figure 2(d) displays hexagonal pattern spots, which can be assigned to the (002), (004) and (006) planes of WS_2. The HRTEM results suggest the as-prepared N–$Co_xW_{1-x}S_2$ also belong to the hexagonal phase and are consistent with the results of XRD and the Raman characterization. It has to be mentioned that although N–$Co_xW_{1-x}S_2$ can be assigned to the hexagonal phase, the lattice parameters have a slight discrepancy with those of hexagonal WS_2. The reason could be ascribed to the incorporation of the N and Co atoms. STEM and EDX-mapping are performed to analyze the elemental distribution, and the results are shown in figure 2(e). Both the linear-scan and mapping scan results show the existence of N, Co, W and S, which are uniformly distributed through the entire nanosheet. Notably, C is also found to be homogeneously distributed on the entire nanosheet. The EDX-mapping demonstrates that the N/Co signals follow the W/S signals. The TEM and HRTEM images of the ultra-thin WS_2 nanosheets and Co_9S_8 nanoparticles are also shown in figure S3.

XPS measurement is carried out to analyze the composition and chemical states of N–$Co_xW_{1-x}S_2$ nanosheets and the obtained spectra of Co 2p, W 4f, S 2p and N 1s are shown in figure S4(a). The Co 2p spectrum displays two doublets of Co^{3+} and Co^{2+}, and two satellites matching well with the reported values of Co 2p [35]. The W 4f spectrum displays

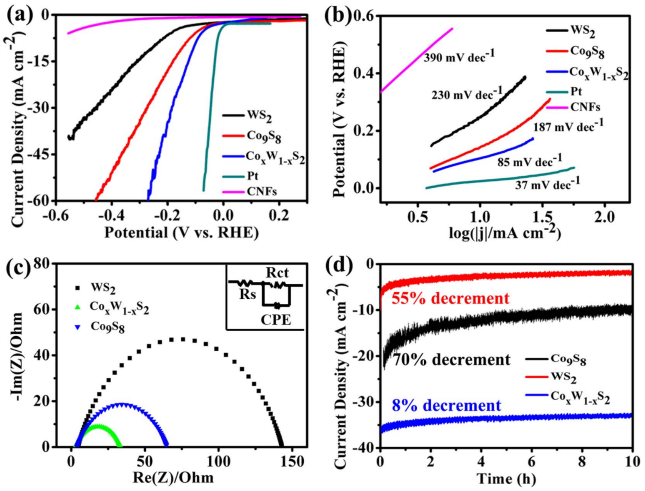

Figure 3. (a) The polarization curves of the samples. (b) The relevant Tafel slope calculated from the LSV curves. (c) The chronoamperometric curves of the obtain samples at the overpotentials of 200 mV. (d) Nyquist plots of the obtained samples.

two sharp peaks at 33.0 and 35.2 eV attributed to the $4f_{7/2}$ and $4f_{5/2}$ of orbitals W^{4+} (figure S4(b)) [36]. Meanwhile, figure S4(c) displays the double major peaks and one shake-up satellite peak appearing at 162.5, 163.7 and 168.5 eV, which are ascribed to the S $2p_{3/2}$ and S $2p_{1/2}$, respectively [37]. Figure S4(d) shows the N 1s spectrum with two peaks, where the N–W bond is distinctly detected at 398.1 eV, demonstrating the presence of N in an obtained solid solution [23].

To investigate the HER activity, the as-prepared samples, were cut into fixed sizes and directly used as the working electrode. As shown in figure 3(a), the Pt/C electrode exhibits the highest current density and lowest onset overpotential towards HER, which is in good agreement with literature results [6]. The N–$Co_xW_{1-x}S_2$ electrode achieves a current density of 10 mA cm^{-2} at a low overpotential of 93 mV, while Co_9S_8 and WS_2 require much higher overpotentials, i.e., 144 mV and 258 mV, respectively. The corresponding Tafel slopes of the electrodes are illustrated in figure 3(b). The N–$Co_xW_{1-x}S_2$ electrode possess a low Tafel slope of 85 mV dec^{-1}, which is approximately 2 times lower than that of Co_9S_8 electrode (187 mV dec^{-1}), and 2.7 times lower than that of WS_2 electrode (230 mV dec^{-1}), suggesting the Volmer–Heyrovsky reaction mechanism [38]. The low Tafel slope indicates that the N–$Co_xW_{1-x}S_2$ electrode has faster HER kinetics than Co_9S_8 and WS_2. The Nyquist plots derived from EIS measurements also demonstrated that the N–$Co_xW_{1-x}S_2$ electrode has faster charge transfer at the electrode surface, evidenced by the smallest charge transfer resistance of 32 Ω, as shown in figure 3(c). The fast charge transfer kinetics of the N–$Co_xW_{1-x}S_2$ electrode is beneficial to the catalytic performance towards HER, which is in good agreement with the polarization curves in figure 3(a).

Long-term stability is also an important parameter for practical applications chronoamperometry measurements were employed to verify the long-term stability of Co_9S_8, WS_2 and N–$Co_xW_{1-x}S_2$ electrode. All the electrodes were fixed at the same overpotentials of –0.200 V for 10 h of operation. As shown in figure 3(d), the chronoamperometric curves demonstrate that the N–$Co_xW_{1-x}S_2$ electrodes possess an excellently stable performance with ca. 8% degradation compared to the initial current. In contrast, the current density of Co_9S_8 and WS_2 sharply decreased by 70% and 55%, respectively. The increased electrochemical stability of the N–$Co_xW_{1-x}S_2$ electrodes is reasonable because the WS_2 nanosheets provide a secure framework for stabilizing the amorphous Co–S clusters and accommodating the presence of the nitrogen anion-decoration. The LSV curves, SEM images and XPS spectrum of the N–$Co_xW_{1-x}S_2$ electrode after long-term stability tests are presented in figure S5, S6 and S7, respectively.

4. Conclusions

In summary, we fabricated nitrogen anion-decorated cobalt tungsten disulfide solid solutions, retaining ultra-thin nanosheet structures anchored on CNFs, to enhance both the catalytic activity and stability via a single facile route. This catalyst shows a significantly promoted HER activity and stable performance compared to pure Co_9S_8 nanoparticles or WS_2 ultra-thin nanosheets. The promoted catalytic activity is reasonable not only because the incorporated Co ion as a promoter reduces the free energy barrier for H adsorption and generates more active sites, leading to better HER activity, but also because accommodating the presence of the nitrogen anion-decoration, which can enhance the electrical conductivity of the catalysts and expedite electron transfer during HER. Meanwhile, WS_2 ultra-thin nanosheets provide a robust framework for stabilizing amorphous Co–S clusters to prevent solubilization in acid solutions. This investigation may provide a feasible strategy for incorporating other heteroatoms into TMDs materials, in order to better design catalysts with highly active and stable performance for water splitting.

Acknowledgments

This study was supported by the National Natural Science Foundation of China (NSFC) (Grant number 51573166).

ORCID iDs

Mingliang Du https://orcid.org/0000-0003-2476-8594

References

[1] Stamenkovic V R, Strmcnik D, Lopes P P and Markovic N M 2016 Energy and fuels from electrochemical interfaces *Nat. Mater.* **16** 57–69
[2] Schlapbach L and Züttel A 2001 Hydrogen storage for mobile applications *Nature* **414** 353–8
[3] Yang Y, Zhang H, Lin Z H, Liu Y, Chen J, Lin Z, Zhou Y S, Wong C P and Wang Z L 2013 A hybrid energy cell for

self-powered water splitting *Energy Environ. Sci.* **6** 2429–34
[4] Park J H, Kim S and Bard A J 2006 Novel carbon-doped TiO_2 nanotube arrays with high aspect ratios for efficient solar water splitting *Nano Lett.* **6** 24–8
[5] An Y R, Fan X L, Luo Z F and Lau W M 2017 Nanopolygons of monolayer MS_2: best morphology and size for HER catalysis *Nano Lett.* **17** 368–76
[6] Wang F *et al* 2015 Enhanced electrochemical H_2 evolution by few-layered metallic $WS_{2(1-x)}Se_{2x}$ nanoribbons *Adv. Funct. Mater.* **25** 6077–83
[7] Li X L *et al* 2017 Strong metal-phosphide interactions in core–shell geometry for enhanced electrocatalysis *Nano Lett.* **17** 2057–63
[8] Carmo M, Fritz D L, Mergel J and Stolten D 2013 A comprehensive review on PEM electrolysis *Int. J. Hydrog. Energy* **38** 4901–34
[9] Wang H, Kong D, Johanes P, Cha J J, Zheng G, Yan K, Liu N and Cui Y 2013 $MoSe_2$ and WSe_2 nanofilms with vertically aligned molecular layers on curved and rough surfaces *Nano Lett.* **13** 3426–33
[10] Kibsgaard J, Jaramillo T F and Besenbacher F 2014 Building an appropriate active-site motif into a hydrogen-evolution catalyst with thiomolybdate $[Mo_3S_{13}]_2$-clusters *Nat. Chem.* **6** 248–53
[11] Li C L, Cao Q, Wang F Z, Xiao Y Q, Li Y B, Delaunay J J and Zhu H W 2018 Engineering graphene and TMDs based van der Waals heterostructures for photovoltaic and photoelectrochemical solar energy conversion *Chem. Soc. Rev.* **47** 4981–5037
[12] Velický M and Toth P S 2017 From two-dimensional materials to their heterostructures: an electrochemist's perspective *Appl. Mater. Today* **8** 68–103
[13] Tan C L *et al* 2017 Recent advances in ultrathin two-dimensional nanomaterials *Chem. Rev.* **117** 6225–331
[14] Ding Q, Song B, Xu P and Jin S 2016 Efficient electrocatalytic and photoelectrochemical hydrogen generation using MoS_2 and related compounds *Chem* **1** 699–726
[15] Voiry D, Salehi M Y, Silva R F, Fujit T H, Chen M W, Asefa T, Shenoy V B, Eda G and Chhowalla M 2013 Conducting MoS_2 nanosheets as catalysts for hydrogen evolution reaction *Nano Lett.* **13** 6222–7
[16] Yang J, Voiry D, Ahn S J, Kang D, Kim A Y, Chhowalla M and Shin H S 2016 Two-dimensional hybrid nanosheets of tungsten disulfide and reduced graphene oxide as catalysts for enhanced hydrogen evolution *Angew. Int., Chem. Ed.* **52** 13751–4
[17] Zhuang M H, Ou X W, Dou Y B, Zhang L L, Zhang Q C, Wu R Z, Ding Y, Shao M H and Luo Z T 2016 Polymer-embedded fabrication of Co_2P nanoparticles encapsulated in N,P-doped graphene for hydrogen generation *Nano Lett.* **16** 4691–8
[18] Jayaramulu K, Masa J, Tomanec O, Peeters D, Ranc V, Schneemann A, Zboril R, Schuhmann W G and Fischer R A 2017 Nanoporous nitrogen-doped graphene oxide/nickel sulfide composite sheets derived from a metal-organic framework as an efficient electrocatalyst for hydrogen and oxygen evolution *Adv. Funct. Mater.* **27** 1700451
[19] Zhang Y S *et al* 2015 Chemical vapor deposition of monolayer WS_2 nano-sheets on Au foils toward direct application in hydrogen evolution *Nano Res.* **8** 2881–90
[20] Zhou H Q, Yu F, Sun J Y, He R, Wang Y M, Guo C F, Wang F, Lan Y C, Ren Z F and Chena S 2016 Highly active and durable self-standing WS_2/graphene hybrid catalysts for the hydrogen evolution reaction *J. Mater. Chem.* A **4** 9472–6
[21] Xing Z C, Yang X R, Asiri A M and Sun X P 2016 Three-dimensional structures of MoS_2@Ni core/shell nanosheets array toward synergetic electrocatalytic water splitting *ACS Appl. Mater. Interfaces* **8** 14521–6
[22] Dai X P, Du K L, Li Z Z, Liu M Z, Ma Y D, Sun H, Zhang X and Yang Y 2015 Co-doped MoS_2 nanosheets with the dominant CoMoS phase coated on carbon as an excellent electrocatalyst for hydrogen evolution *ACS Appl. Mater. Interfaces* **7** 27242–53
[23] Sun C Q, Zhang J Y, Ma J, Liu P, Gao D Q, Tao K and Xue D S 2016 N-doped WS_2 nanosheets: a high-performance electrocatalyst for the hydrogen evolution reaction *J. Mater. Chem.* A **4** 11234–8
[24] Ming F W, Liang H F, Shi H H, Xu X, Mei G and Wang Z C 2016 MOF-derived Co-doped nickel selenide/C electrocatalysts supported on Ni foam for overall water splitting *J. Mater. Chem.* A **4** 15148–55
[25] Lim D, Hwang H, Kim T, Shim S E and Baeck S H 2015 Fabrication and characterization of amorphous cobalt-doped molybdenum sulfide for hydrogen evolution reaction *J. Nanosci. Nanotechnol.* **15** 8257
[26] Bonde J, Moses P G, Jaramillo T F, Norskov J K and Chorkendorff I 2009 Hydrogen evolution on nano-particulate transition metal sulfides *Faraday Discuss.* **140** 219–31
[27] Tran P D, Chiam S Y, Boix P P, Ren Y, Praman S S, Fize J, Artero V and Barber J 2013 Novel cobalt/nickel-tungsten-sulfide catalysts for electrocatalytic hydrogen generation from water *Energy Environ. Sci.* **6** 2452–9
[28] Anitha V P, Major S, Chandrashekharam D and Bhatnagar M 1996 Deposition of molybdenum nitride thin films by r.f. reactive magnetron sputtering *Surf. Coat. Technol.* **79** 50–4
[29] Chakrapani V, Thangala J and Sunkara M K 2009 WO_3, and W_2N nanowire arrays for photoelectrochemical hydrogen production *Int. J. Hydrog. Energy* **34** 9050–9
[30] Chen P Z, Zhou T P, Chen M L, Tong Y, Zhang N, Peng X, Chu W S, Wu X J, Wu C Z and Xie Y 2017 Enhanced catalytic activity in nitrogen-anion modified metallic cobalt disulfide porous nanowire arrays for hydrogen evolution *ACS Catal.* **7** 7405–11
[31] Shannon R D 1976 Crystal physics, diffraction, theoretical and general *Acta Cryst.* **A32** 751–66
[32] Hou Y, Wen Z, Cui S, Ci S, Mao S and Chen J 2015 An advanced nitrogen-doped graphene/cobalt-embedded porous carbon polyhedron hybrid for efficient catalysis of oxygen reduction and water splitting *Adv. Funct. Mater.* **25** 872–82
[33] Shifa T A, Wang F, Liu K, Xu K, Wang Z, Zhan X, Jiang C and He J 2016 Engineering the electronic structure of 2D WS_2 nanosheets using Co incorporation as $Co_xW_{(1-x)}S_2$ for conspicuously enhanced hydrogen generation *Small* **12** 3802–9
[34] Zhang Y *et al* 2013 Controlled growth of high-quality monolayer WS_2 layers on sapphire and imaging its grain boundary *ACS Nano* **7** 8963–71
[35] Sivanantham A, Ganesan P and Shanmugam S 2016 Hierarchical $NiCo_2S_4$ nanowire arrays supported on Ni foam: an efficient and durable bifunctional electrocatalyst for oxygen and hydrogen evolution reactions *Adv. Funct. Mater.* **26** 4661–72
[36] Zou M L, Zhang J F, Zhu H, Du M L, Wang Q F, Zhang M and Zhang X 2015 A 3D dendritic WSe_2 catalyst grown on carbon nanofiber mats for efficient hydrogen evolution *J. Mater. Chem.* A **3** 12149–53
[37] Duan J, Chen S, Chambers B A, Andersson G G and Qiao S Z 2015 3D WS_2 nanolayers@heteroatom-doped graphene films as hydrogen evolution catalyst electrodes *Adv. Mater.* **27** 4234–41
[38] Zheng Y, Jiao Y, Jaroniec M and Qiao S Z 2015 Advancing the electrochemistry of the hydrogen evolution reaction through combining experiment and theory *Angew. Chem., Int. Ed.* **54** 52–65